Exciton–Plasmon Coupling Enhancement *via* Metal Oxidation

Francesco Todisco,[†,‡,⊥] Stefania D'Agostino,[§,⊥] Marco Esposito,[†,‡] Antonio I. Fernández-Domínguez,[#] Milena De Giorgi,[*,†] Dario Ballarini,[†] Lorenzo Dominici,[†,§] Iolena Tarantini,[‡] Massimo Cuscuná,[†] Fabio Della Sala,[§,∥] Giuseppe Gigli,[†,‡] and Daniele Sanvitto[†]

[†]CNR NANOTEC, Istituto di Nanotecnologia Polo di Nanotecnologia c/o Campus Ecotekne, Via Monteroni Lecce, Via Monteroni, Lecce, Italy 73100, [‡]Dipartimento di Matematica e Fisica "Ennio De Giorgi" Strada Provinciale Lecce-Monteroni, Universitá del Salento, Campus Ecotekne, Lecce, Italy 73100, [§]Center for Biomolecular Nanotechnologies@UNILE, Istituto Italiano di Tecnologia, Via Barsanti, Arnesano, Italy 73010, [#]Departamento de Fisica Teòrica de la Materia Condensada and Condensed Matter Physics Center (IFIMAC), Universidad Autònoma de Madrid Calle Francisco Tomás y Valiente, 7 Madrid, Spain E-28049, and [∥]Istituto Nanoscienze, CNR, Euromediterranean Center for Nanomaterial Modelling and Technology (ECMT), Via Arnesano, Lecce, Italy 73100. [⊥]F. Todisco and S. D'Agostino contributed equally.

ABSTRACT In this paper, we report on the effect of metal oxidation on strong coupling interactions between silver nanostructures and a J-aggregated cyanine dye. We show that metal oxidation can sensibly affect the plexcitonic system, inducing a change in the coupling strength. In particular, we demonstrate that the presence of oxide prevents the appearance of Rabi splitting in the extinction spectra for thick spacers. In contrast, below a threshold percentage, the oxide layer results in an higher coupling strength between the plasmon and the Frenkel exciton. Contrary to common belief, a thin oxide layer seems thus to act, under certain conditions, as a coupling mediator between an emitter and a localized surface plasmon excited in a metallic nanostructure. This suggests that metal oxidation can be exploited as a means to enhance light–matter interactions in strong coupling applications.

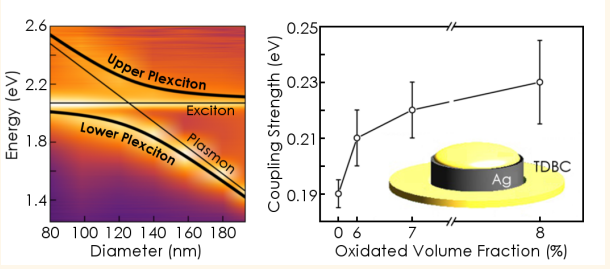

KEYWORDS: plasmon · plexciton · strong coupling · oxidation · Rabi splitting

Metal nanostructures have a number of optical properties that are crucial for their integration in a new generation of active nanophotonic devices.[1−4] Plasmons, *i.e.*, the collective oscillations of electrons at the boundary between a metal and a dielectric material, have already shown their unique optical properties, such as extreme light amplification in the near-field,[5] high sensitivity to the surrounding environment,[6−8] and subwavelength mode volume.[9,10] Despite all these properties, the extremely weak plasmon nonlinearities put an important limitation on the integration of metallic nanostructures as active components in nano-optical circuits.[11−13] This limitation can be overcome by combining the optical properties of metals with those of organic/inorganic materials, exploiting both the small plasmonic mode volume and the high excitonic nonlinearities. For this reason, in the last years a great interest was devoted to the study of interactions between localized plasmons and nanoscale components, including organic molecules. Interesting phenomena have been demonstrated in these kinds of systems, used in a wide range of technological applications, such as surface-enhanced Raman spectroscopy,[14] nanoscale lasers,[15] plasmon-enhanced light harvesting and photocatalysis,[16] and ultrasensitive chemical and biological sensing.[17] In view of these and other applications involving plasmon–molecule interactions, the physics of the electromagnetic (EM) coupling between a plasmonic mode and an excitonic oscillating dipole deserves to be deeply investigated. Usually the coupling is such that only the spontaneous emission rate of the emitters is modified, the exciton and plasmon frequency remaining unaltered (weak-coupling regime).[18] However, it can also happen that the coupling strength between the EM mode and the exciton is stronger than absorption and radiative losses. In this case the energy levels of the whole system are also modified (strong coupling regime), and the

* Address correspondence to milena.degiorgi@nano.cnr.it.

Received for review April 14, 2015 and accepted September 17, 2015.

Published online September 17, 2015
10.1021/acsnano.5b04974

plasmon−exciton interaction results in the formation of light−matter mixture energy states, called plexcitons.[19] As a result, two new branches arise in the modal dispersion curves, characterized by an anticrossing behavior and separated by the so-called Rabi splitting.[20]

Recently, strong coupling has been reported for surface plasmon polaritons[21−25] and localized plasmons[26−30] interacting with an ensemble of molecular J-aggregates,[26,27] dyes,[28−30] or semiconductor nanocrystals.[25,31] In particular, Frenkel excitons in organic semiconductors show very large oscillator strengths even at room temperature. This results in a stronger interaction of such excitons with EM modes, compared to their inorganic counterparts.[32] Both arrays[26,30,33] and single[19,34] metal nanostructures have been studied, and strong coupling has also been observed in the presence of surface lattice resonances in ordered nanoparticle arrays.[35] Interestingly, it has been shown that spatially coherent hybrid states emerge when a set of molecular emitters and surface plasmons enter the strong coupling regime.[36,37] Finally, much experimental[38,39] and theoretical[40] interest has also been focused lately on the impact of the inclusion of a passive spacer layer in the plasmon−exciton coupling in hybrid J-aggregate and metal nanoparticle systems, making possible a control of the electric field distribution and the plasmonic extinction.

Localized plasmons are typically exploited, at optical frequencies, by using silver or gold nanoparticles. In particular, silver presents remarkable properties, which have been used in plasmonic designs featuring large absorption cross section[41] and yielding strong near-field enhancement.[42] Moreover silver, if compared to gold, allows the realization of lower losses and cheaper devices[43] with resonances in the visible spectral range. Unfortunately, however, silver is also more prone to oxidation than gold. The presence of oxide, in fact, strongly affects the plasmonic response of silver nanoparticles, resulting in the red-shift of their spectral resonances and the decrease of extinction efficiency.[44−46] Recently it has been demonstrated that silver nanoparticle degradation can be highly slowed down either by a thiol surface coating[47] or contacting them with cobalt nanoparticles.[48]

Here we investigate how metal oxide growth on silver nanodisks, usually unavoidable in practical systems, affects their strong near-field interaction with a molecular J-aggregated dye. Surprisingly, we find that, in the regime of small oxidation, the presence of Ag_2O appears beneficial rather than detrimental, in the increase of the plasmon−exciton coupling strength as a function of the oxide percentage. This counterintuitive behavior is shown experimentally and interpreted by two theoretical models that attribute such an effect to modal volume decrease and plasmonic losses reduction. The theoretical analysis is based on both numerical simulations, performed in the framework of the discrete dipole approximation (DDA), and an analytical model able to give a qualitative estimation of the coupling strength trend as a function of the nanoparticle oxidation degree. We believe that our findings could open new avenues in a conscious and advantageous exploitation of oxidation in practical systems.

RESULTS AND DISCUSSION

Silver nanodisks (NDs) are defined by electron beam lithography on a quartz substrate. Several squared arrays of equally spaced 70 × 70 NDs are fabricated with 40 nm height, diameters ranging from 50 to 190 nm, and a side-by-side interparticle distance twice the ND diameter, so as to simultaneously minimize near-field interactions between neighbor nanoparticles[49] and maintain a constant ND fill factor. Figure 1a shows the results of extinction measurements performed on a confocal setup, as a function of the ND diameter. The colors indicate the measured extinction in linear scale from minimum (black) to maximum (white). An extinction peak is clearly visible for each array, whose spectral position shifts from 1.58 eV to 2.84 eV as the ND diameter decreases from 177 nm to 57 nm. The resonance spectral position can be fitted with a linear function, plotted as a solid line in Figure 1a. The sample is conserved in a vacuum chamber (10 mbar) so as to slow down the metal oxidation process, and it is measured in air, at room temperature. In Figure 1b we show the plasmon energy, full width at half-maximum (fwhm), and extinction peak value after one, two, and five aging days in the vacuum chamber, for an array of NDs with 116 nm diameter. It is evident that the plasmon resonance broadens, undergoes a red-shift, and decreases in the extinction efficiency with increasing time.

The plasmon−exciton coupled system is obtained by spin coating a thin film of a J-aggregated cyanine dye (5,5′,6,6′-tetrachloro-1,1′-diethyl-3,3′-di(4-sulfobutyl)-benzimidazolocarbocyanine, or TDBC). By AFM measurements on a scratched part of the sample, we estimated a film thickness of 15 ± 5 nm. For such a hybrid system a clear three-peak feature is observed in the extinction spectra, as shown in Figure 1c. Here the sharp extinction peak at 2.07 eV corresponds to absorption from the uncoupled J-aggregated TDBC. The other two peaks in the spectra are characterized by a clear anticrossing as a function of the ND diameter. This behavior is characteristic of the strong coupling regime and reveals the formation of two new mixed states, *i.e.*, the upper (UP) and lower (LP) plexciton branches.

The measured extinction spectra, recorded at different aging times, are fitted with a two-coupled-oscillators model, characterized by the Hamiltonian

$$H = \begin{pmatrix} E_{pl}(t,d) - i\gamma_{pl}(t,d) & g(t) \\ g(t) & E_{exc} - i\gamma_{exc} \end{pmatrix} \quad (1)$$

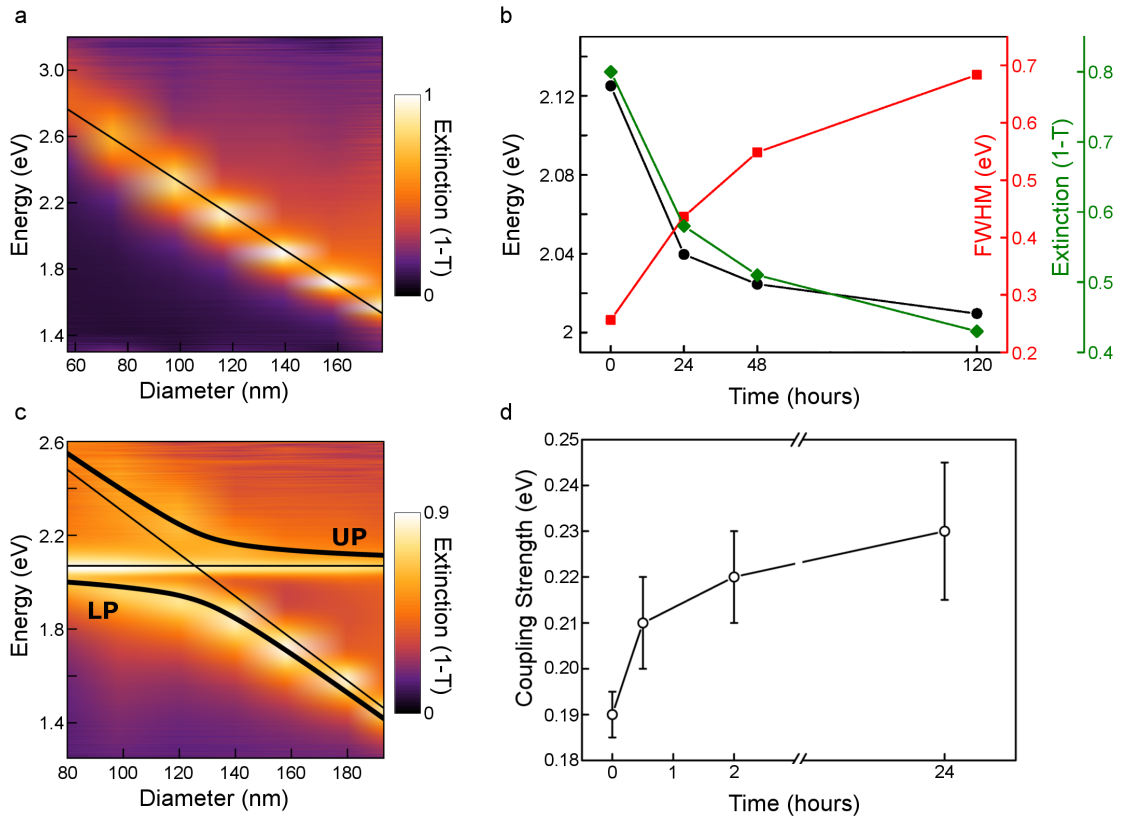

Figure 1. (a) As fabricated silver ND extinction map as a function of ND diameter. The colors render the measured extinction in linear scale from minimum (black) to maximum (white), as shown in the color legend. The plasmon resonance red-shifts with increasing ND diameter and can be well fitted by a linear function, shown as a solid line in the map. (b) Plasmon energy (black circles), full width at half-maximum (red squares), and extinction peak value (green rhombus) as a function of aging time for an array of NDs with 116 nm diameter, taken as reference. The same trend is measured for the other ND diameter arrays. (c) Experimental extinction map of the as-fabricated plasmon−exciton coupled system, showing an anticrossing behavior between the upper and lower plexciton branches. The dispersion is fitted with a two-coupled-oscillators model (thick lines), by using the plasmon energy dispersion calculated from the bare plasmon measurements and the exciton energy at 2.07 eV (thin lines). (d) Coupling strength extracted from fitting the dispersion curves at all aging times. The error bars of the extracted coupling strength increase with aging time as a consequence of the oxidation-driven plasmon broadening. After 1 day aging the spectra broadening is so large that they cannot be fitted anymore.

Here E_{pl} is the plasmon energy as a function of the nanodisk diameter d, obtained through the linear fit of the bare plasmon spectra for different aging times t, E_{exc} is the uncoupled exciton energy (2.07 eV), and g is the coupling strength, left as a free parameter, and equal to half the Rabi splitting at the plasmon−exciton energy crossing point (zero detuning condition). γ_{exc} and γ_{pl} are the exciton and plasmon homogeneous line widths, respectively. The former is equal to 32 meV, as obtained by fitting the experimental absorption spectra, while the latter is evaluated from numerical simulations for a single ND, as a function of the ND diameter. By solving eq 1 and fitting the experimental energy dispersions in Figure 1c and Figure S1, the coupling strength g was extracted as a function of the aging time. Note that since the oxidation process results in the red-shift of the plasmonic resonances, the zero-detuning condition at which the coupling strength is extracted also shifts toward smaller ND diameter at increasing aging times. The results are shown in Figure 1d. Surprisingly, we found the coupling strength to increase from 190 meV to 230 meV during the first 24 h of aging, which indicates a stronger plasmon−exciton interaction for an oxidation factor, as discussed below, less than 6%. At longer aging times, random oxidation (see Figure S1) results in a large inhomogeneity across the array of NDs, and the plasmon resonance broadens. As a result, even if the zero detuning condition is still satisfied with smaller NDs, the splitting visibility rapidly decreases after 24 h, and the coupling strength cannot be extracted anymore (see Figure S3).

To shed light on the oxidation process of silver antennas, a numerical investigation is performed within the DDA scheme, by using the ADDA code.[50] Maxwell equations are solved for an isolated disk geometry only. We neglect collective effects associated with the diffractive coupling among different elements of the disk arrangement. This is justified by the fact that we are only interested in the coupling strength, which is not influenced by diffraction effects and given the

inherent spatially incoherent nature of the J-aggregate emission across the experimental samples. Metal oxidation is a random process that results in the irregular growth of oxide around the metal nanostructures (see Figure S1).[51] For this reason, it is not possible to define a precise geometry for the oxidized nanoparticles. Therefore, Ag NDs lying on a SiO_2 substrate are simulated keeping a constant geometry and increasing the oxide percentage inside the nanostructures by using the Maxwell–Garnett approach,[52] similarly to what was recently done for other Ag and Al nanoparticles.[53,54] The metal-oxide effective dielectric function is then obtained by solving the equation

$$\frac{\varepsilon_{\text{eff}} - \varepsilon_{\text{m}}}{\varepsilon_{\text{eff}} + 2\varepsilon_{\text{m}}} = F\,\frac{\varepsilon_{\text{ox}} - \varepsilon_{\text{m}}}{\varepsilon_{\text{ox}} + 2\varepsilon_{\text{m}}} \qquad (2)$$

Here ε_{m}, ε_{ox}, and ε_{eff} are the metal, oxide (that we assumed to be Ag_2O, which is more stable at room temperature[55]), and effective metal-oxide dielectric functions, respectively, and F is the oxide volume fraction to be calculated ($V_{Ag_2O}/V_{\text{Disk}}$). The permittivities of Ag and Ag_2O used in our calculations are taken from experimental data.[56,57]

Simulations are performed by using a plane wave polarized in the plane of the substrate as incident field. The spectral positions of the simulated extinction peaks are thus compared with the experimental ones, and the oxide volume fraction inside the NDs at each aging time is extracted. As shown in Figure 2 for a 116 nm diameter ND, percentages of 6%, 7%, and 8% are found to match the experimental results at 24, 48, and 120 h aging times, respectively. Note that the measured spectra for oxidized NDs are broader than the theoretical ones. This can be caused by structural inhomogeneities across the experimental samples, not reproduced in the single disk calculations, and clearly shown in Figure S1. On the contrary, for as-fabricated NDs the experimental peak is sharper than the theoretical one because of diffraction effects induced by the array periodicity. In the inset a SEM image of as-fabricated 190 nm diameter NDs is reported.

To numerically reproduce the plexcitonic features, we include in the DDA simulation a TDBC layer covering the Ag ND lying on the infinite SiO_2 substrate. In this regard we consider the complex dielectric function of the J-aggregated dye to be modeled by a Lorentzian line shape:

$$\varepsilon_{\omega} = \varepsilon_{\infty} - f\,\frac{{\omega_{\text{exc}}}^2}{\omega^2 - {\omega_{\text{exc}}}^2 + i\gamma_{\text{exc}}\omega} \qquad (3)$$

with the high-frequency component ε_{∞}, the reduced oscillator strength f, the exciton line width γ_{exc}, and the transition energy $\hbar\omega_{\text{exc}}$ taken from ref 26 and fixed to $\varepsilon_{\infty} = 2.56$, $f = 0.41$, $\gamma_{\text{exc}} = 0.03$ eV, and $\hbar\omega_{\text{exc}} = 2.07$ eV, respectively. Through a systematic numerical investigation, it is found that the experimental results are nicely reproduced by including a 10 nm thick TDBC layer covering the NDs. In particular, by assuming the geometry shown in the sketch of Figure 3a, the agreement between the experimental and numerical spectra is satisfactory, as demonstrated in Figure 3a. Note that the molecule extinction peak appears more intense in the experimental measurements due to the huge amount of uncoupled molecules in the whole illuminated area, while simulations are, instead, performed on a finite-sized target.

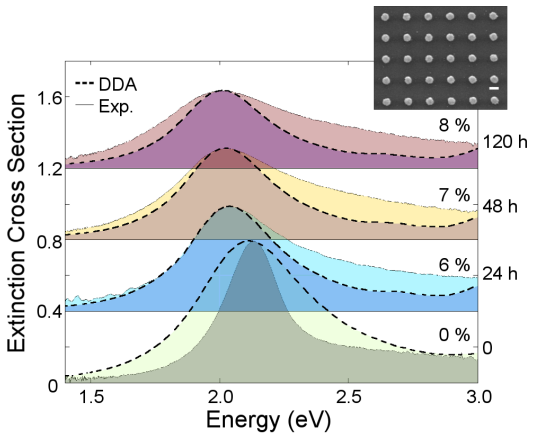

Figure 2. Effect of oxidation on optical properties of silver NDs. Comparison between the experimental (solid) and the theoretical (dashed) extinction peak for a 116 nm diameter ND. Simulated peaks were obtained by using a metal-oxide effective medium dielectric function calculated with the Maxwell–Garnett approximation. By comparing the energy position of the peaks, oxide volume percentages of 6%, 7%, and 8% were found to fit the experimental data for 24, 48, and 120 h aging times, respectively. In the inset, a SEM image of as-fabricated 190 nm diameter silver NDs is shown (scale bar: 200 nm).

To analyze the effects of the oxide layer in terms of plasmon–exciton coupling, the total decay rate of a dipole Γ normalized to its free-space value, Γ_0, is computed by exciting variously oxidized NDs with point-like dipole sources located 5 nm away from their surface (corresponding to the middle of the TDBC layer) and oscillating at the exciton energy (2.07 eV). The oscillating dipoles are assumed to have two in-plane orientations (P_x and P_y) and are moved along the profile of the NDs in the regions covered by the TDBC, as shown in the schematic drawing in Figure 3b. Here we show that a slight oxidation of the metallic nanostructure generates an enhancement of the total decay rate perturbation Γ/Γ_0 and thus of the normalized photonic density $\rho(\mathbf{r}_i, \omega_{\text{exc}})$ at position $\mathbf{r}_i$ occupied by the dipoles and at excitation frequency ω_{exc}.

By averaging on all the considered dipole geometries, in terms of orientations (k) and position (i), we calculate the mean value of the normalized photonic density for each oxide volume fraction:

$$\overline{\rho}_{\omega_{\text{exc}}} = \frac{1}{2N}\sum_{k=1}^{2}\sum_{i=1}^{N}\rho_k(\mathbf{r}_i, \omega_{\text{exc}}) \qquad (4)$$

These values, reported in the inset of Figure 4a, reveal that the presence of a small percentage of Ag_2O induces an increase in ρ, compared to the pure Ag case ($F = 0$).

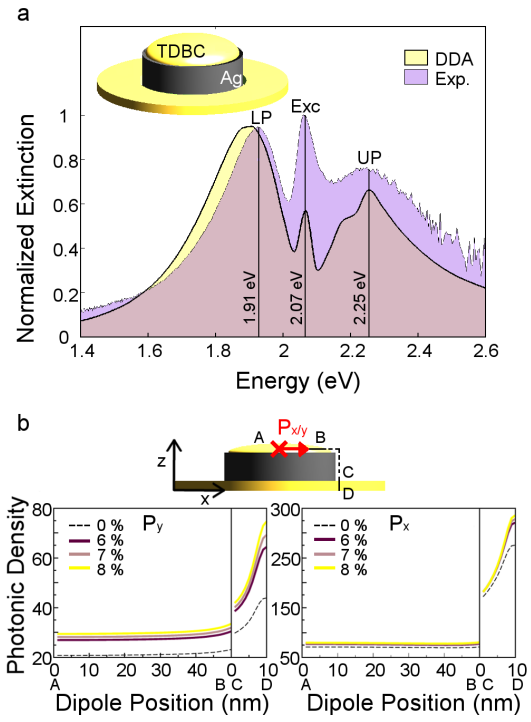

Figure 3. (a) Experimental (violet) and calculated (yellow) extinction spectra for a TDBC covered, 116 nm diameter Ag ND, with the geometry shown in the inset. The characteristic three-peak feature of a strongly coupled system is clearly visible, *i.e.*, the lower and upper polariton branches and the uncoupled exciton (LP, UP, and Exc, respectively). (b) Normalized photonic density around variously oxidized silver NDs. The nanoantenna (a 116 nm diameter ND) is excited by a point-like emitter located at 5 nm from the surface and oscillating, with an energy of 2.07 eV, along the *y* (left) and *x* (right) direction. The normalized photonic density is then calculated as the total decay rate of the dipole normalized to its free-space value, and it is reported as a function of the emitter position for the four degrees of oxidation, corresponding to the aged samples in Figure 2 (0%, 6%, 7%, and 8%).

This can be explained by considering the change induced in the *effective* dielectric function of the ND by the presence of the oxide and thus in the resonant behavior that the dipole polarizability of the ND displays for a fixed energy (2.07 eV). The change in the Ag dielectric function induced by the presence of oxide, in fact, results in reduced absorption losses in the metal at the exciton frequency and hence in a lower plasmon damping. A test performed using the Fröhlich condition yields a peak similar to the one in the inset of Figure 4a, shifted at smaller *F*, this probably being due to retardation effects beyond the quasi-static approximation (see Supporting Information, Figure S3).

It can be shown that the calculation of the normalized photonic density $\rho(\mathbf{r}_i, \omega_{exc})$, which involves the rigorous solution of Maxwell equations in DDA, can be correlated to the equivalent quantity in the quantum model of light−matter interaction and thus to the coupling parameter g through the simple relation[58,59]

$$g(\mathbf{r}_i, \omega_{exc}) = (\Gamma_0 \gamma_{pl}(\rho(\mathbf{r}_i, \omega_{exc}) - 1)/4)^{1/2} \qquad (5)$$

where $\Gamma_0 = \gamma_{exc}$ is the excitonic spontaneous decay rate in the absence of the metallic nanoparticle and γ_{pl} is the plasmon homogeneous line width extracted from the DDA extinction spectra obtained for each oxidation factor *F*. The electromagnetic coupling between the plasmon and the exciton is a local phenomenon to be analyzed point-to-point. Anyway a mean value $\bar{g}$ can be extracted by considering an averaging procedure similar to the one in eq 4. The mean values obtained for g span from 0.17 eV at 0% of oxide to 0.215 eV at 20%, as shown in Figure 4a. Note that, despite the arbitrary choice of the distance between the emitter and the ND (fixed to 5 nm), our calculations well reproduce

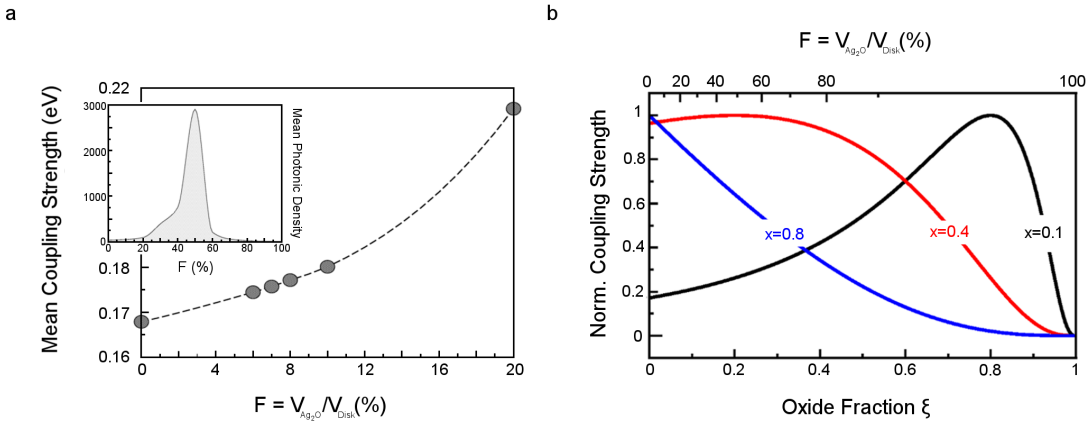

Figure 4. (a) Mean coupling strength as a function of the oxidation factor *F*, calculated within the DDA framework. The mean values are extracted, for a low degree of oxidation, from the mean photonic density shown in the inset. This has been calculated by fixing the emitter frequency to the TDBC emission maximum (2.07 eV) and its distance from the nanoparticle surface to 5 nm. Simulations were performed for two in-plane orientations of the dipole surce (P_x and P_y) and for all the positions, along the disk profile, occupied by TDBC. Reported values are the mean values. (b) Normalized coupling strength reported as a function of the oxide fraction ξ (bottom scale) or of the oxidation factor *F* (top scale), for $h/a = 0.08$, calculated by applying a modified geometry for the system reported in refs 60 and 61. Three different values of the parameter *x* are shown: *x* = 0.1 (black line), 0.4 (red line), and 0.8 (blue line).

- the value of the Rabi splitting extracted from Figure 1c ($2g$ = 0.38 eV), being $\bar{g}_{F=0\%}$ = 0.17 eV;
- the increasing trend of the coupling strength experimentally observed for this oxidation range and reported in Figure 1d.

To gain more physical insight into this counterintuitive behavior, found both experimentally and numerically, we developed a simple analytical model, able to qualitatively describe the coupling strength of the oxidized system, by means of geometrical and oxide electromagnetic screening effect considerations. Recently, Delga *et al.*[60,61] have shown that the coupling strength g_l between a quantum emitter (QE) and the localized plasmonic mode of angular momentum l supported by a metal nanosphere can be expressed in analytical form in the quasi-static regime. Note that although the quasi-static approximation does not allow for an accurate description of the extinction characteristics of hybrid organometallic systems whose size is comparable to the incident wavelength,[40,62] it has been successfully applied to the treatment of high-order plasmonic modes in different contexts,[63] even beyond the purely static regime through the so-called radiative reaction concept.[64,65] Taking this into account, in our minimal model, built for qualitative purposes only, we assume that the theory developed for nanometric spherical geometries in refs 60 and 61 is valid for our ∼100 nm sized NDs-on-a-substrate experimental samples. Importantly, these assumptions are only justified because, as shown below, this model reproduces the general trend dependence of the coupling strength on the oxidation level observed in experiments and simulations. This way, dropping all the terms except for the geometrical parameters, we supposed, to a first approximation, that the coupling strength corresponding to the dipolar plasmon mode in our plexcitonic system can be written as

$$g_{l=1} \propto \left(\frac{1}{a^3 \left(1+\frac{h}{a}\right)^{2+4}} \right)^{1/2} = \left(\frac{a^3}{(a+h)^6} \right)^{1/2} \quad (6)$$

where a is the ND radius and h is the distance between the J-aggregate position and the metal surface.

To apply this analytical model to our system, we assume that the oxidation effectively reduces the size of the nanoparticle by a fraction ξ (between 0 and 1, where ξ = 0 means no oxidation, while ξ = 1 means total oxidation) of the initial dimension a. In this way, the nanostructure can be considered as an effective core−shell metal-oxide system, with $(1 - \xi)a$ and ξa the metallic core and the oxide shell dimensions, respectively. Moreover, in order to take into account the optical response of the grown oxide, we introduce an effective distance between the QE and the nanoparticle, which weights the oxide contribution with a constant parameter x. That is, we replaced $(a + h)$ in the denominator with $[a(1 - \xi) + h + x\xi a]$. Finally, as already shown in the literature, a dielectric shell surrounding a metal nanoparticle or flat surface introduces a cutoff limit in the parallel wave-vectors that can be excited in the system at a given frequency.[66−68] In our NDs, we assume that this effect prevents the excitation of higher order multipole (l > 1) plasmon modes and that only the dipole l = 1 contributes to the emitter−ND coupling. We thus write the total coupling strength in our system as

$$g\left(\xi, \frac{h}{a}, x\right) \propto \left(\frac{(1-\xi)^3}{\left[(1-\xi)+\frac{h}{a}+x\xi\right]^6} \right)^{1/2} \equiv \tilde{g} \quad (7)$$

In Figure 4b we plot $\tilde{g}$ normalized to 1, as a function of the oxide fraction ξ for three different values of the parameter x (0.1, 0.4, and 0.8). The ratio h/a is assumed to be fixed to 0.086 (being a = 58 nm and h = 5 nm) near the detuning zero condition. As a result, the model shows that for high values of x (x > 0.5), $\tilde{g}$ is a monotonically decreasing function, as we expected. For lower values, on the other hand, $\tilde{g}$ always converges toward zero for a completely oxidized nanoparticle, but with a nonmonotonic trend, thus suggesting that moderate values of the parameter x (below 0.5) can well describe our system. Note that we have built an analytical minimal model for the coupling strength dependence on the oxidation fraction, based on three assumptions: the validity of the quasi-static picture, the fact that the dipolar plasmonic mode governs the exciton−plasmon coupling, and the negligible role played by the metallic shape (spherical/cylindrical). These approximations allow us not only to reproduce qualitatively our experimental and numerical observations but also to gain physical insight into our findings. These can now be explained in the following way. On one hand an increase of the oxide fraction induces an increase of the effective distance between the QE and the metallic nanoantenna, which would simply result in the decrease of the coupling strength (as shown by the monotonic drops of the normalized coupling strength, for high x values, in Figure 4b). On the other hand, for small values of x (<0.5), this extra distance can effectively be compensated by the penetration of the plasmon into the oxide layer more than it would do in a vacuum. At the same time, the oxidation results in a reduction of the nanoparticle dimension, which, in turn, leads to a smaller effective modal volume with a consequently higher coupling to the molecular dipole.

The numerical and analytical models thus confirm, from two different perspectives, that the effect of low oxide fractions in silver nanostructures is not detrimental for the onset of the strong light−matter coupling regime, but, on the contrary, it can actually help. The presence of oxide, both as an impurity/host

material inside the ND (numerical approach) and as an external layer corroding the ND edges (analytical approach) results, thus, in an effective increase of the radiative decay channel of the localized plasmons excited inside the metallic antennas.

CONCLUSIONS

In conclusion, this work shows that, below a threshold volume fraction, silver oxide can act as a coupling mediator between an emitter and a localized surface plasmon excited in a metallic nanostructure, and thus it behaves as an intensifier of light−matter interaction for strong coupling applications. The results shown here open a new surprising scenario in which the presence of a small quantity of oxide does not prevent the appearance of Rabi splitting in extinction spectra, but instead favors it.

METHODS

Sample Fabrication. Two-dimensional ND arrays were fabricated by electron beam lithography on a glass substrate. After cleaning the substrate in acetone and 2-propanol, a 250 nm poly(methyl methacrylate) (PMMA) layer was spin coated on glass at 6000 rpm and soft-baked at 180 °C for 3 min. Subsequently, a chrome layer 2 nm thick was thermally evaporated to prevent charge effects. The arrays were written by a Raith 150 system at 22 pA beam current and 30 keV. After electron exposure, the Cr layer was removed by a ceric ammonium nitrate based wet etcher for 20 s and rinsed in water. The exposed resist was development in MIBK:IPA solution in a 1:3 ratio for 3 min and rinsed in 2-propanol for 1 min. After thermal evaporation of 40 nm of silver, a liftoff process was performed in an mr-Rem 500 remover solution (Microresist Technology) and rinsed in 2-propanol.

For the molecule interacting system, a 1 mg/mL solution of TDBC in methanol was prepared and filtered. Then dichloromethane was added in a 1:2 volume ratio. The resulting solution was finally spin coated onto the whole sample at 2000 rpm.

Optical Characterization. Extinction spectra were measured on a confocal setup. Light from a tungsten lamp was focused on the sample with a condenser (NA < 0.1) and collected with a 10× objective lens (NA 0.45). Transmitted light was then spatially selected and focused on the slits of a monochromator coupled to a CCD camera.

Numerical Simulations. Version 1.3 of the open-source code ADDA developed by Yurkin and Hoekstra[50] was used. The main feature of ADDA is the ability to run on a multiprocessor system by parallelizing a single DDA simulation. For what concerns the choice of the interdipole distance or discretization parameter d_{int} (which in DDA represents the side of the elementary cube), all the results were obtained by setting d_{int} = 1 nm, which, for the large targets analyzed here, was enough to ensure convergence. The perturbations on the dipole total decay rate induced by the plasmons were analyzed in the framework of the DDA, and further details on the method can be found in ref 69.

Conflict of Interest: The authors declare no competing financial interest.

Supporting Information Available: The Supporting Information is available free of charge on the ACS Publications website at DOI: 10.1021/acsnano.5b04974.

Additional figures and numerical simulations (PDF)

Acknowledgment. This work has been partially founded by the ERC project POLAFLOW (Grant No. 308136) and the national project "Molecular nAnotechnologies for eAlth and environmenT" (MAAT, PON02_00563_3316357 and CUP B31C12001230005) for financial support. We thank P. Cazzato for technical support, E. Del Valle and A. González-Tudela for beneficial discussions, and G. Accorsi for organic materials assistance and characterization.

REFERENCES AND NOTES

1. Maier, S. A. *Plasmonics Fundamentals and Applications*; Springer: New York, 2007.
2. Ozbay, E. Plasmonics: Merging Photonics and Electronics at Nanoscale Dimensions. *Science* **2006**, *311*, 189–193.
3. Barnes, W. L.; Dereux, A.; Ebbesen, T. W. Surface Plasmon Subwavelength Optics. *Nature* **2003**, *424*, 824–830.
4. Large, N.; Abb, M.; Aizpurua, J.; Muskens, O. L. Photoconductively Loaded Plasmonic Nanoantenna as Building Block for Ultracompact Optical Switches. *Nano Lett.* **2010**, *10*, 1741–1746.
5. Schuller, J. A.; Barnard, E. S.; Cai, W.; Jun, Y. C.; White, J. S.; Brongersma, M. L. Plasmonics for Extreme Light Concentration and Manipulation. *Nat. Mater.* **2010**, *9*, 193–204.
6. McFarland, A. D.; Van Duyne, R. P. Single Silver Nanoparticles as Real-Time Optical Sensors with Zeptomole Sensitivity. *Nano Lett.* **2003**, *3*, 1057–1062.
7. Zhao, J.; Xiaoyu, Z.; Ranjit Yonzon, C.; Haes, A. J.; Van Duyne, R. P. Localized Surface Plasmon Resonance Biosensors. *Nanomedicine* **2006**, *1*, 219–228.
8. Anker, J. N.; Hall, W. P.; Lyandres, O.; Shah, N. C.; Zhao, J.; Van Duyne, R. P. Biosensing with Plasmonic Nanosensors. *Nat. Mater.* **2008**, *7*, 442–453.
9. Miyazaki, H. T.; Kurokawa, Y. Squeezing Visible Light Waves into a 3-nm-Thick and 55-nm-Long Plasmon Cavity. *Phys. Rev. Lett.* **2006**, *96*, 097401.
10. Ciraci, C.; Hill, R. T.; Mock, J. J.; Urzhumov, Y.; Fernández-Domínguez, A. I.; Maier, S. A.; Pendry, J. B.; Chilkoti, A.; Smith, D. R. Probing the Ultimate Limits of Plasmonic Enhancement. *Science* **2012**, *337*, 1072–1074.
11. Huck, A.; Witthaut, D.; Kumar, S.; Sørensen, A. S.; Andersen, U. L. Large Optical Nonlinearity of Surface Plasmon Modes on Thin Gold Films. *Plasmonics* **2013**, *8*, 1597–1605.
12. MacDonald, K. F.; Sámson, Z. L.; Stockman, M. I.; Zheludev, N. I. Ultrafast Active Plasmonics. *Nat. Photonics* **2009**, *3*, 55–58.
13. Pacifici, D.; Lezec, H. J.; Atwater, H. A. All-Optical Modulation by Plasmonic Excitation of CdSe Quantum Dots. *Nat. Photonics* **2007**, *1*, 402–406.
14. Fang, Y.; Seong, N.-Y.; Dlott, D. D. Measurement of the Distribution of Site Enhancements in Surface-Enhanced Raman Scattering. *Science* **2008**, *321*, 388–392.
15. Noginov, M. A.; Zhu, G.; Belgrave, A. M.; Bakker, R.; Shalaev, V. M.; Narimanov, E. E.; Stout, S.; Herz, E.; Suteewrong, T.; Wiesner, U. Demonstration of a Spaser-Based Nanolaser. *Nature* **2009**, *460*, 1110–1112.
16. Standridge, S. D.; Schatz, G. C.; Hupp, J. T. Distance Dependence of Plasmon-Enhanced Photocurrent in Dye-Sensitized Solar Cells. *J. Am. Chem. Soc.* **2009**, *131*, 8407–8409.
17. Kabashin, A. V.; Evans, P. R.; Pastkovsky, S.; Hendren, W.; Wurtz, G. A.; Atkinson, R.; Pollard, R. J.; Podolskiy, V. A.; Zayats, A. V. Plasmonic Nanorod Metamaterials for Biosensing. *Nat. Mater.* **2009**, *8*, 867–871.
18. Akselrod, G. M.; Argyropoulos, C.; Hoang, T. B.; Ciracì, C.; Fang, C.; Huang, J.; Smith, D. R.; Mikkelsen, M. H. Probing the Mechanisms of Large Purcell Enhancement in Plasmonic Nanoantennas. *Nat. Photonics* **2014**, *8*, 835–840.
19. Schlather, A. E.; Large, N.; Urban, A. S.; Nordlander, P.; Halas, N. J. Near-Field Mediated Plexcitonic Coupling and Giant Rabi Splitting in Individual Metallic Dimers. *Nano Lett.* **2013**, *13*, 3281–3286.
20. Törmä, P.; Barnes, W. L. Strong Coupling between Surface Plasmon Polaritons and Emitters. *Rep. Prog. Phys.* **2015**, *78*, 013901.

21. Dintinger, J.; Klein, S.; Bustos, F.; Barnes, W.; Ebbesen, T. Strong Coupling between Surface Plasmon-Polaritons and Organic Molecules in Subwavelength Hole Arrays. *Phys. Rev. B: Condens. Matter Mater. Phys.*. **2005**, *71*. DOI: 10.1103/PhysRevB.71.035424
22. Bellessa, J.; Bonnand, C.; Plenet, J.; Mugnier, J. Strong Coupling between Surface Plasmons and Excitons in an Organic Semiconductor. *Phys. Rev. Lett.* **2004**, *93*. DOI: 10.1103/PhysRevLett.93.036404
23. Symonds, C.; Bellessa, J.; Plenet, J. C.; Brehier, A.; Parashkov, R.; Lauret, J. S.; Deleporte, E. Emission of Hybrid Organic-Inorganic Exciton/Plasmon Mixed States. *Appl. Phys. Lett.* **2007**, *90*, 091107.
24. Passmore, B. S.; Adams, D. C.; Ribaudo, T.; Wasserman, D.; Lyon, S.; Davids, P.; Chow, W. W.; Shaner, E. A. Observation of Rabi Splitting from Surface Plasmon Coupled Conduction State Transitions in Electrically Excited InAs Quantum Dots. *Nano Lett.* **2011**, *11*, 338–342.
25. Gomez, D. E.; Lo, S. S.; Davis, T. J.; Hartland, G. V. Picosecond Kinetics of Strongly Coupled Excitons and Surface Plasmon Polaritons. *J. Phys. Chem. B* **2013**, *117*, 4340–4346.
26. Bellessa, J.; Symonds, C.; Vynck, K.; Lemaitre, A.; Brioude, A.; Beaur, L.; Plenet, J. C.; Viste, P.; Felbacq, D.; Cambril, E.; et al. Giant Rabi Splitting between Localized Mixed Plasmon-Exciton States in a Two-Dimensional Array of Nanosize Metallic Disks in an Organic Semiconductor. *Phys. Rev. B: Condens. Matter Mater. Phys.* **2009**, *80*, 033303.
27. Fofang, N. T.; Park, T.-H.; Neumann, O.; Mirin, N. A.; Nordlander, P.; Halas, N. J. Plexcitonic Nanoparticles Plasmon-Exciton Coupling in Nanoshell-J-Aggregate Complexes. *Nano Lett.* **2008**, *8*, 3481–3487.
28. Wurtz, G. A.; Evans, P. R.; Hendren, W.; Atkinson, R.; Dickson, W.; Pollard, R. J.; Zayats, A. V.; Harrison, W.; Bower, C. Molecular Plasmonics with Tunable Exciton-Plasmon Coupling Strength in J-Aggregate Hybridized Au Nanorod Assemblies. *Nano Lett.* **2007**, *7*, 1297–1303.
29. Sugawara, Y.; Kelf, T. A.; Baumberg, J. J.; Abdelsalam, M. E.; Bartlett, P. N. Strong Coupling between Localized Plasmons and Organic Excitons in Metal Nanovoids. *Phys. Rev. Lett.* **2006**, *97*, 266808.
30. Cade, N. I.; Ritman-Meer, T.; Richards, D. Strong Coupling of Localized Plasmons and Molecular Excitons in Nanostructured Silver Films. *Phys. Rev. B: Condens. Matter Mater. Phys.* **2009**, *79*, 241404.
31. Gomez, D. E.; Vernon, K. C.; Mulvaney, P.; Davis, T. J. Surface Plasmon Mediated Strong Exciton-Photon Coupling in Semiconductor Nanocrystals. *Nano Lett.* **2010**, *10*, 274–278.
32. Berrier, A.; Cools, R.; Arnold, C.; Offermans, P.; Crego-Calama, M.; Brongersma, S. H.; Gòmez-Rivas, J. Active Control of the Strong Coupling Regime between Porphyrin Excitons and Surface Plasmon Polaritons. *ACS Nano* **2011**, *5*, 6226–6232.
33. Salomon, A.; Wang, S.; Hutchison, J. A.; Genet, C.; Ebbesen, T. W. Strong Light-Molecule Coupling on Plasmonic Arrays of Different Symmetry. *ChemPhysChem* **2013**, *14*, 1882–1886.
34. Zengin, G.; Johansson, G.; Johansson, P.; Antosiewicz, T. J.; Käll, M.; Shegai, T. Approaching the Strong Coupling Limit in Single Plasmonic Nanorods Interacting with J-Aggregates. *Sci. Rep.* **2013**, *3*. DOI: 10.1038/srep03074
35. Väkeväinen, A. I.; Moerland, R. J.; Rekola, H. T.; Eskelinen, A.-P.; Martikainen, J.-P.; Kim, D.-H.; Törmä, P. Plasmonic Surface Lattice Resonances at the Strong Coupling Regime. *Nano Lett.* **2014**, *14*, 1721–1727.
36. Aberra Guebrou, S.; Symonds, C.; Homeyer, E.; Plenet, J. C.; Gartstein, Y. N.; Agranovich, V. M.; Bellessa, J. Coherent Emission from a Disordered Organic Semiconductor Induced by Strong Coupling with Surface Plasmons. *Phys. Rev. Lett.* **2012**, *108*, 066401.
37. Shi, L.; Hakala, T. K.; Rekola, H. T.; Martikainen, J.-P.; Moerland, R. J.; Törmä, P. Spatial Coherence Properties of Organic Molecules Coupled to Plasmonic Surface Lattice Resonances in the Weak and Strong Coupling Regimes. *Phys. Rev. Lett.* **2014**, *112*, 153002.
38. Yoshida, A.; Uchida, N.; Kometani, N. Synthesis and Spectroscopic Studies of Composite Gold Nanorods with a Double-Shell Structure Composed of Spacer and Cyanine Dye J-Aggregate Layers. *Langmuir* **2009**, *25*, 11802–11807.
39. Yoshida, A.; Yonezawa, Y.; Kometani, N. Tuning of the Spectroscopic Properties of Composite Nanoparticles by the Insertion of a Spacer Layer: Effect of Exciton-Plasmon Coupling. *Langmuir* **2009**, *25*, 6683–6689.
40. Lebedev, V. S.; Medvedev, A. S. Optical Properties of Three-Layer Metal-Organic Nanoparticles with a Molecular J-Aggregate Shell. *Quantum Electron.* **2013**, *43*, 1065.
41. Link, S.; El-Sayed, M. A. Spectral Properties and Relaxation Dynamics of Surface Plasmon Electronic Oscillations in Gold and Silver Nanodots and Nanorods. *J. Phys. Chem. B* **1999**, *103*, 8410–8426.
42. Erol, M.; Han, Y.; Stanley, S. K.; Stafford, C. M.; Du, H.; Sukhishvili, S. SERS Not To Be Taken for Granted in the Presence of Oxygen. *J. Am. Chem. Soc.* **2009**, *131*, 7480–7481.
43. Wang, F.; Shen, Y. R. General Properties of Local Plasmons in Metal Nanostructures. *Phys. Rev. Lett.* **2006**, *97*, 206806.
44. Lok, C.-N.; Ho, C.-M.; Chen, R.; He, Q.-Y.; Yu, W.-Y.; Sun, H.; Tam, P. K.-H.; Chiu, J.-F.; Che, C.-M. Silver Nanoparticles: Partial Oxidation and Antibacterial Activities. *JBIC, J. Biol. Inorg. Chem.* **2007**, *12*, 527–534.
45. Yin, Y.; Li, Z.-Y.; Zhong, Z.; Gates, B.; Xia, Y.; Venkateswaran, S. Synthesis and Characterization of Stable Aqueous Dispersions of Silver Nanoparticles through the Tollens Process. *J. Mater. Chem.* **2002**, *12*, 522–527.
46. D'Agostino, S.; Sala, F. D. Active Role of Oxide Layers on the Polarization of Plasmonic Nanostructures. *ACS Nano* **2010**, *4*, 4117–4125.
47. Qi, H.; Alexson, D. A.; Glembocki, O. J.; Prokes, S. M. Synthesis and Oxidation of Silver Nanoparticles *Proc. SPIE* **2011**, .79470Y
48. Sachan, R.; Ramos, V.; Malasi, A.; Yadavali, S.; Bartley, B.; Garcia, H.; Duscher, G.; Kalyanaraman, R. Oxidation-Resistant Silver Nanostructures for Ultrastable Plasmonic Applications. *Adv. Mater.* **2013**, *25*, 2045–2050.
49. Su, K.-H.; Wei, Q.-H.; Zhang, X.; Mock, J. J.; Smith, D. R.; Schultz, S. Interparticle Coupling Effects on Plasmon Resonances of Nanogold Particles. *Nano Lett.* **2003**, *3*, 1087–1090.
50. Yurkin, M. A.; Hoekstra, A. G. The Discrete-Dipole-Approximation Code ADDA: Capabilities and Known Limitations. *J. Quant. Spectrosc. Radiat. Transfer* **2011**, *112*, 2234−2247. Code available at http://code.google.com/p/a-dda/.
51. Sun, L.; Noh, K. W.; Wen, J.-G.; Dillon, S. J. In Situ Transmission Electron Microscopy Observation of Silver Oxidation in Ionized/Atomic Gas. *Langmuir* **2011**, *27*, 14201–14206.
52. Garnett, J. C. M. Colours in Metal Glasses and in Metallic Films. *Philos. Trans. R. Soc., A* **1904**, *203*, 385–420.
53. Kuzma, A.; Weis, M.; Flickyngerova, S.; Jakabovic, J.; Satka, A.; Dobrocka, E.; Chlpik, J.; Cirak, J.; Donoval, M.; Telek, P.; et al. Influence of Surface Oxidation on Plasmon Resonance in Monolayer of Gold and Silver Nanoparticles. *J. Appl. Phys.* **2012**, *112*, 103531.
54. Knight, M. W.; King, N. S.; Liu, L.; Everitt, H. O.; Nordlander, P.; Halas, N. J. Aluminum for Plasmonics. *ACS Nano* **2014**, *8*, 834–840.
55. De Rooij, A. The Oxidation of Silver by Atomic Oxygen. *EsA J.* **1989**, *13*, 363–382.
56. Palik, E. D. *Handbook of Optical Constants of Solids*; Academic Press, 1998.
57. Xiao-Yong, G.; Hong-Liang, F.; Jiao-Min, M.; Zeng-Yuan, Z. Spectroscopic Ellipsometric Study of the Optical Properties of Ag2O Film Prepared by Direct-Current Magnetron Reactive Sputtering. *Chin. Phys. B* **2010**, *19*, 090701.
58. Savasta, S.; Saija, R.; Ridolfo, A.; Di Stefano, O.; Denti, P.; Borghese, F. Nanopolaritons: Vacuum Rabi Splitting with a Single Quantum Dot in the Center of a Dimer Nanoantenna. *ACS Nano* **2010**, *4*, 6369–6376.
59. Lambropoulos, P. *Fundamentals of Quantum Optics and Quantum Information*; Springer: Berlin, 2007.
60. Delga, A.; Feist, J.; Bravo-Abad, J.; Garcia-Vidal, F. J. Quantum Emitters Near a Metal Nanoparticle: Strong

Coupling and Quenching. *Phys. Rev. Lett.* **2014**, *112*, 253601.
61. Delga, A.; Feist, J.; Bravo-Abad, J.; Garcia-Vidal, F. J. Theory of Strong Coupling between Quantum Emitters and Localized Surface Plasmons. *J. Opt.* **2014**, *16*, 114018.
62. Lebedev, V. S.; Medvedev, A. S. Plasmon-Exciton Coupling Effects in Light Absorption and Scattering by Metal/J-Aggregate Bilayer Nanoparticles. *Quantum Electron.* **2012**, *42*, 701–713.
63. Pendry, J. B.; Fernández-Domínguez, A. I.; Luo, Y.; Zhao, R. Capturing Photons with Transformation Optics. *Nat. Phys.* **2013**, *9*, 518–522.
64. Aubry, A.; Lei, D. Y.; Maier, S. A.; Pendry, J. B. Conformal Transformation Applied to Plasmonics beyond the Quasi-static Limit. *Phys. Rev. B: Condens. Matter Mater. Phys.* **2010**, *82*, 205109.
65. Carminati, R.; Greffet, J.-J.; Henkel, C.; Vigoureux, J. M. Radiative and Non-Radiative Decay of a Single Molecule Close to a Metallic Nanoparticle. *Opt. Commun.* **2006**, *261*, 368–375.
66. Peña-Rodríguez, O.; Pal, U. Effects of Surface Oxidation on the Linear Optical Properties of Cu Nanoparticles. *J. Opt. Soc. Am. B* **2011**, *28*, 2735–2739.
67. Strashko, A.; Agranovich, V. To the Theory of Surface Plasmon-Polaritons on Metals Covered with Resonant Thin Films. *Opt. Commun.* **2014**, *332*, 201–205.
68. González-Tudela, A.; Huidobro, P. A.; Martín-Moreno, L.; Tejedor, C.; García-Vidal, F. J. Reversible Dynamics of Single Quantum Emitters Near Metal-Dielectric Interfaces. *Phys. Rev. B: Condens. Matter Mater. Phys.* **2014**, *89*, 041402.
69. D'Agostino, S.; Della Sala, F.; Andreani, L. C. Dipole-Excited Surface Plasmons in Metallic Nanoparticles: Engineering Decay Dynamics within the Discrete-Dipole Approximation. *Phys. Rev. B: Condens. Matter Mater. Phys.* **2013**, *87*. DOI: 10.1103/PhysRevB.87.205413